Mn *K*-edge XANES study of the $La_{1-x}Ca_xMnO_3$ colossal magnetoresistive manganites

A. Yu. Ignatov* and N. Ali
Department of Physics, Southern Illinois University, Carbondale, Illinois 62901

S. Khalid
National Synchrotron Light Source, Brookhaven National Laboratory, Upton, New York 11973
(Received 28 June 2000; revised manuscript received 10 November 2000; published 12 June 2001)

We report Mn *K*-edge x-ray absorption near edge structure (XANES) calculations of the $La_{1-x}Ca_xMnO_3$ manganites considering three pair correlations, according to the three fundamental degrees of freedom governing their unusual electronic properties, namely, the electronic structure of the unoccupied states probed by the Mn *K*-edge profile versus (i) local atomic distortions; (ii) local magnetic ordering; and (iii) the charge-transfer nature of the Mn-O bonds. The calculations are accompanied by Mn *K*-edge XANES measurements in the temperature range 30–300 K. The main features of the absorption edge can be qualitatively reproduced in terms of single-electron multiple-scattering calculations for an 87-atom cluster. Lattice polaronic distortions in $La_{0.7}Ca_{0.3}MnO_3$ are simulated assuming a strongly distorted orthorhombic structure above and an almost undistorted rhombohedral structure below T_c. The results roughly reproduce the energy ''shift'' across T_c observed experimentally. Mn *K*-edge spin-polarized XANES spectra of the $x=0$, 0.3, and 1 samples are presented. An energy splitting between the majority- and minority-spin spectra of 0.5–1.1 eV contributes to the total XANES broadening below the Néel (Curie) temperature. A small feature B_3 standing approximately 6 eV above the main absorption peak is beyond the scope of single-electron calculations; it is assigned to a shake-up transition. To illustrate, the calculated Mn *K* edge is obtained as the convolution product of the single-electron XANES and the spectrum of many-body excitations in the Mn-O electronic states upon the sudden switching on of the Mn 1*s* core hole. We investigate the charge-transfer (CT) versus. Mott-Hubbard-type ground state using the U_d, Δ, and the T_{dp} parameters determined by previous Mn $2p$ x-ray photoemission spectroscopy measurements and find that $LaMnO_3$ should be viewed as a CT-type insulator with a substantial O $2p$ component in the ground state. In light of these results the controversial issue of Mn valence states in the manganites is critically reexamined. We argue that the disproportionation may be understood as a mixture of the CT many-body electronic configurations coupled with spin and lattice degrees of freedom.

DOI: 10.1103/PhysRevB.64.014413 PACS number(s): 78.70.En, 61.10.Ht, 78.70.Dm, 75.70.Pa

I. INTRODUCTION

More than 40 years after their discovery[1] the $La_{1-x}Ca_xMnO_{3+\delta}$ perovskites have attracted renewed interest, especially due to their interesting electronic, magnetic, and structural properties as well as for their potential technological applications. The term ''colossal magnetoresistance'' (CMR) was introduced recently to describe the large temperature and magnetic field dependences of the resistivity in $La_{1-x}A_xMnO_{3+\delta}$ ($A=Ca,Sr,Ba$) perovskites. The detailed phase diagram of $La_{1-x}Ca_xMnO_3$ is still not clear, presenting one of the challenges in the field. $LaMnO_3$ is an antiferromagnetic (AFM) insulator with ferromagnetic (FM) coupling in the MnO_2 planes and AFM coupling between the planes.[2] With Ca doping ($0.2<x<0.5$) the system exhibits a paramagnetic to ferromagnetic transition on cooling that is accompanied by a metal to insulator (MI) transition. For higher Ca concentrations the ground state is AFM (Ref. 2) and nonmetallic.[1] Samples with $0.5<x<0.7$ exhibit charge ordering (CO).[3,4]

The main focus of experimental and theoretical work has been on the metallic CMR materials ($0.2<x<0.5$) whose transport properties and FM ordering at low temperatures are understood in terms of the double-exchange (DE) mechanism proposed by Zener.[5] Substitution of La^{3+} by Ca^{2+} in $LaMnO_3$ converts some of the Mn^{3+} ions into Mn^{4+}. Electron hopping between Mn^{3+} and Mn^{4+} neighbors through the O^{-2} is enhanced if the ionic spins are aligned ferromagnetically, thereby favoring low resistivity and a ferromagnetic ground state at low temperatures. It has been realized recently that the DE (Ref. 5) or extended DE (Ref. 6 and 7) mechanisms are not the only physics controlling the properties of the CMR materials. Millis *et al.*[8] argued that conventional DE is not enough to explain the resistivity data and suggested that a lattice effect must be present to reduce the kinetic energy of the carriers at the MI transition. The atomic displacements are implicitly included in the model[9] giving rise to a strong coupling of the carriers to Jahn-Teller lattice distortions. There is also convincing experimental evidence that the strong coupling impacts both the carriers[10,11] and the lattice.[12–14] The former includes, but is not limited to, a giant isotope effect[10] and the sign anomaly of the Hall effect.[11] The latter has been established by locally sensitive techniques, such as extended x-ray absorption fine structure (EXAFS) measurements[12,13] and neutron diffraction pair distribution function (PDF) analysis,[14] showing the Mn-O bonds to be strongly distorted above T_c. In addition to the electron-lattice coupling spin-lattice coupling has been proposed[15] to explain the high insulatorlike resistivity above the transition temperature and the large CMR effect. Hundley *et al.*[16] have

pointed out that the resistance relates to the magnetization as $\ln(\rho)\sim -M$. Booth *et al.*[12] found a functional relation between the magnetization and the number of delocalized holes per Mn site n_{dh}, $\ln(n_{dh})\sim M$, suggesting that as a trapped hole becomes delocalized it no longer contributes to the Mn-O distortions.

It is worth mentioning that in Zener's picture the hopping occurs through a nominally closed shell O^{2-}, i.e., the oxygen band does not play an active role in the DE. It was pointed out by Pickett and Singh[17] that the Mn $d-$O p hybridization is much too strong to be considered perturbatively through the closed O shell. O *K*-edge electron-energy-loss spectra[18] (EELS) and x-ray absorption near edge structure (XANES) measurements[19,20] have confirmed that the manganites are charge-transfer (CT) insulators within the scheme by Zaanen, Sawatzky, and Allen,[21] similar to the higher-temperature Cu-based superconductors. EELS and XANES spectra show an unsplit doublet (CT peak at $E\sim 528$ eV and upper Hubbard band peak at $E\sim 530$ eV) corresponding to the O $2p$ unoccupied density of states. The CT peak systematically increases in intensity within the range of Sr doping until $x<0.3$ (Ref. 18) [$x<0.4$ (Ref. 20)] and presumably in the $0<x<0.7$ range of Ca doping in $LaMnO_3$.[19] Remarkably, there is a striking correlation between EELS and resistivity data: the larger the O $2p$ hole density, the smaller the resistivity. This implies that the conductivity is hole driven and the O $2p$ holes contribute significantly to the conduction mechanism, including the magnetoresistance.[18] Photoemission spectroscopy and O *K*-edge XANES results[22] support the charge-transfer-type model of $La_{1-x}Sr_xMnO_3$. The ground state of $LaMnO_3$ is found to be a mixture of d^4 and d^5L configurations (here L denotes an O ligand hole). Holes doped into $LaMnO_3$ spread between the many-body configurations but they are mainly of O $2p$ character.

One of the constituents of the Mn $3d-$O $2p$ hybridization—the Mn valence—has been the subject of many controversial conclusions.[23] This question can be worthily addressed by x-ray absorption near-edge structure spectroscopy. Being a fast and locally sensitive technique, XANES can provide information on local atomic and local electronic structures. The Mn *K*-edge XANES that is employed as an experimental tool in this study is due to a dipole transition of the $1s$ core-hole electron to the p-like unoccupied density of states[24] (DOS) projected on to the Mn absorbing site. Since the $4p$ Mn states are strongly hybridized with O $2p$ and Mn $3d$ states of the neighboring atoms, the local p-like projected density of states is very sensitive to the charge distribution and local distortions of Mn-O bonds, as well as to any variations in Mn $3d-$O $2p$ hybridization that is believed to form the electronic states near the Fermi energy. It should be noted that the electronic structure of the manganites is an extraordinarily complicated many-body problem that is governed by a strong interplay between three fundamental degrees of freedom: lattice, spin, and electronic.[25] In this paper we adopt a simplified approach, considering three pair correlations (according to the three fundamental degrees of freedom), namely, the electronic structure of the unoccupied states (probed by the Mn *K*-edge profile) vs (i) local atomic distortions; (ii) local magnetic ordering; and (iii) Mn $3d-$O $2p$ hybridization.

Before going into details of our calculations let us briefly consider the most important results in the Mn *K*-edge absorption measurements[12,26–30] following our chosen classification. Local lattice distortions as the reason for the changes in the Mn *K*-edge XANES spectrum of $La_{0.75}Ca_{0.25}MnO_3$ have been discussed by Lanzara *et al.*[26] They found a correlation between the energy shift of the Mn *K*-edge and the average Mn-O distance deduced from their quantitative Mn *K*-edge EXAFS analysis.[13] In this paper we present a detailed analysis of lattice effects on the Mn *K*-edge spectra of $La_{1-x}Ca_xMnO_3$.

Mn *K*-edge studies were attempted to deduce the role of the local magnetic ordering through temperature-dependent measurements across the ferromagnetic-to-paramagnetic phase transition[12,27,28] and field-dependent measurements.[27] It is worth mentioning that conventional XANES is not directly sensitive to the ferromagnetic ordering or to the antiferromagnetic/ferromagnetic ordering as are x-ray magnetic circular dichroism (XMCD) and spin-polarized XANES (SPXANES). The temperature dependence of the Mn *K*-edge spectra shows very minor changes in the Mn electronic states of $La_{0.6}Y_{0.07}Ca_{0.33}MnO_3$.[27] These changes are expressed in terms of a chemical shift that is about one order of magnitude larger in the paramagnetic phase than in the ferromagnetic phase. In contrast to Ref. 27, Bridges *et al.*[28] have reported that most of the changes in the main edge of $La_{0.79}Ca_{0.21}MnO_3$ occur in the temperature range below T_c. The origin of these changes in the XANES spectra is not specified in either work and calls for further evaluations.

Most XANES work is focused on the electronic states of the Mn ions, i.e., on the Mn valence problem. Subías *at al.*[27] have attempted to fit the Mn *K*-edge data ($x=0.33$) to a sum of two edges: 67% of $LaMnO_3$ and 33% of $CaMnO_3$. The large discrepancy between the experimental spectrum and the model is indicative of an intermediate oxidation state for the Mn ion, which does not fluctuate between pure ionic Mn^{3+} and Mn^{4+}. Only one type of manganese is present in $La_{1-x}Ca_xMnO_3$.[27] Systematic shifts in the absorption position of the Mn *K* edge with doping have been reported in Refs. 12, 27 and 29. From the Mn *K*-edge XANES measurements Croft *et al.*[29] have emphasized that the formal Mn^{3+} and Mn^{4+} states in $La_{1-x}Ca_xMnO_3$ do not correspond to the pure ionic $3d^4$ and $3d^3$ states. The Mn $3d$ hole response to Ca substitution is delayed up to $x\sim 0.2$. For more highly doped compounds $3d$ (presumably e_g) hole formation is strongly suggested.[29] Electron diffraction measurements[3] give supporting evidence for real space charge ordering in the range $0.63<x<0.67$ at low temperature. However, Mn still acts as if mixed valent on the time scale of $\sim 10^{-15}$ s in the $x=0.65$ sample according to Mn *K*-edge data.[12] Very recently Qian *et al.*[30] have come forward with the notion that a mixing of covalent Mn d configurations should be considered instead of a single Mn configuration[30] in order to ascertain the charge/orbital ordering. From the temperature dependent Mn K_β emission and Mn *K*-edge absorption measurements of the $x=0.5$ and $x=0.5,0.65$ samples, respectively, one can infer a slight increase in the average Mn valence at low temperatures. Changes in the balance of the

thermal energy, Jahn-Teller, (JT) local distortion, ferromagnetic/antiferromagnetic ordering, and charge-ordered interaction energies at fixed composition x can alter the balance of the Mn configurations and, therefore, alter the effective average Mn valence in the system.[30]

Summarizing these results, Mn fluctuations have been considered in the framework of Mn $3d$ configurations with different hole numbers at the Mn sites.[12,27–30] In a wider sense, to the best of our knowledge, the question of Mn $3d$–O $2p$ hybridization was not thoroughly discussed so far in work on the Mn K edge. The O $2p$ band was completely ignored resulting in several drawbacks, which we will discuss in Sec. VI C. Perhaps the most striking of them is a limiting of the possible candidates for the ground state to a mixture of Mn $3d$ configurations, implying an essentially Mn $3d$ character of the doped states. To clarify the nature of valence fluctuations in the manganites we need an in-depth understanding of how the Mn $3d$–O $2p$ hybridization affects the Mn K-edge profile. If the holes predominantly reside on the O sites[18–20] will the Mn K-edge measurements be sensitive to this type of charge transfer?

Although previous XANES work has established general trends in the composition-dependent behavior of the Mn K edge and ruled out the pure ionic Mn valences of $+2$, $+3$, and $+4$ in the doped CMR materials, several fundamental questions remain. Experimental measurements were not accompanied by any theoretical calculations. We still lack information on the origin of the features arising at the Mn K edge and their responses to changes in the electronic and local structure of the CMR materials. In this paper we report Mn K-edge XANES calculations for several members of the $La_{1-x}Ca_xMnO_3$ family, aiming at revealing the effects of (i) local lattice distortions, (ii) local magnetic ordering, and (iii) the covalent nature of the Mn-O bonds on the shape of the Mn K-edge. Once these questions are answered, one might expect to gain a better understanding of the controversial issue of Mn valence from Mn K-edge analysis.

II. EXPERIMENT

Powder samples of $La_{1-x}Ca_xMnO_{3+\delta}$ ($x=0$, 0.15, 0.2, 0.3, 0.4, 0.5, 0.67, and 1.0) were prepared by the standard solid-state reaction at temperatures up to 1480 °C ($T=1480-150x$) depending on composition. The firing temperatures were chosen to keep $\delta=0.03$ all through the series.[31] Two oxygen-rich samples of $LaMnO_{3+\delta}$ ($\delta\sim0.07$ and 0.15) were prepared by carrying out the two final sinterings at 1380 and 1200°C.

X-ray powder diffraction patterns were measured from all samples using a Rigaku diffractometer. The complete patterns were analyzed by the Rietveld method using the GSAS code.[32] All samples, except for $LaMnO_{3.15}$, were refined in terms of the orthorhombic space group $Pbnm$, consistent with previous diffraction measurements. $LaMnO_{3.15}$ belongs to the rhombohedral R-$3c$ space group. No secondary phases were revealed. Fluorescent microprobe analysis showed good space homogeneity of the samples.

Magnetic properties were investigated using a commercial Quantum Design quantum interference device magnetometer. $LaMnO_{3+\delta}$, $\delta=0.03$ and $\delta\sim0.15$, exhibit antiferromagnetic and ferromagnetic transitions at $T_N\sim140$ K and $T_c\sim160$ K. Metallic samples with $x=0.15$, 0.2, 0.3, and 0.4 show ferromagnetic-to-paramagnetic phase transitions on warming. At the applied magnetic field of 1 kOe the estimated transition temperatures are 170, 183, 230, and 241 K, respectively. The magnetization of the $x=0.67$ sample behaves consistently with a charge-ordering transition at $T_{CO}\sim270$ K and an antiferromagnetic transition at ~140 K.[3] Pure $CaMnO_3$ is antiferromagnetic below $T_N\sim130$ K. For resistivity measurements several pellets were cut into bars and four wires were attached with silver skin. The $La_{0.7}Ca_{0.3}MnO_3$ sample showed a sharp metal-to-insulator phase transition on warming at $T\sim210$ K. For the $La_{0.33}Ca_{0.67}MnO_3$ sample $d\rho(T)/dT<0$ up to the maximum available temperature of 400 K. However, resistivity abruptly increases at $T\sim T_{CO}$ in agreement with results of Ref. 33

Mn K-edge spectra were collected at beamlines X-19A and X-18B at the National Synchrotron Radiation Light Source using a Si(111) double-crystal monochromators. Experimental runs at X-19A and X-18B revealed essentially identical results for the same samples after bringing the spectra to an absolute energy scale. Strictly speaking, the energy resolutions were a slightly bit different, although better than 1 eV in both cases. For this reason we will always refer to the experimental data recorded at one of the beamlines: either X-19A for $x=0.3$ or X-18B for the $x=0.67$ sample while discussing small temperature-dependence variations in the pre-edge range ($E\sim6542$ eV). The higher-order harmonics were suppressed by detuning the second crystal of the monochromator on its rocking curve to 50% of the maximum transmitted intensity at 300 eV above the edge. Spectra were recorded simultaneously in the fluorescent yield (FY) and the transmission modes (TM). In order to suppress the remaining La L_1-edge oscillations we used a 13-element Ge detector (Canberra) with an energy resolution of 180 eV. The Mn K_γ fluorescent detection ($E=5.898$ keV) reduces the contribution from the La L edges, although the suppression is not complete because the La L_γ fluorescent line is confined in the energy window of the Ge detector. The sample in the He cryostat was oriented to have the incident x-ray striking the surface at $45°\pm5°$ and the exit angle of the fluorescent x rays was $\sim45°\pm10°$. This geometry provided essentially bulk-sensitive FY measurements.[34] In order to calibrate the energy scale a pure Mn foil was placed between the second and third ion chambers as a standard. Following Croft *et al*,[29] relative energies between different spectra were obtained by careful comparison of the standard data. After all spectra were put onto the same relative scale the absolute energy scale was calibrated by assigning $E=6539.1$ eV to the first inflection point of the pure Mn foil.

Generally, from three to six scans at each temperature point for each sample were taken to improve the signal-to-noise ratio. The total FY counts were not smaller than $(1-2)\times10^5$ at the top of the absorption edge ($E\sim6550-6555$ eV), providing a typical error in the measured intensity at a level below 1% for the low intense pre-edge

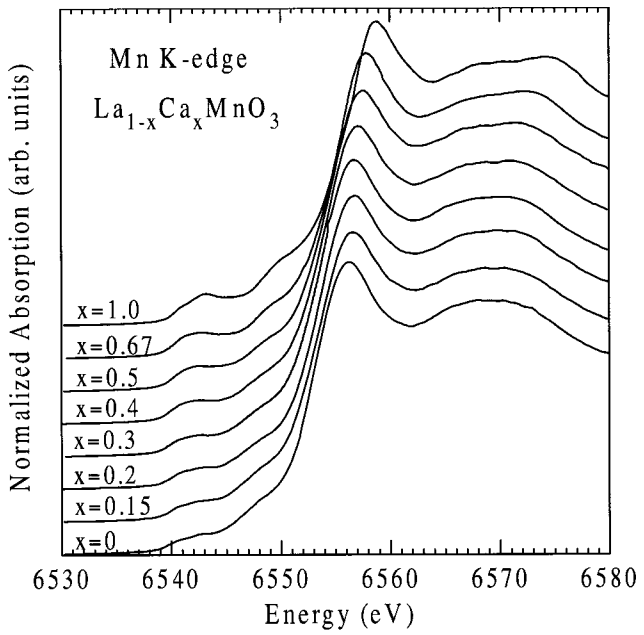

FIG. 1. Evolution of the Mn *K*-edge spectra with x in the $La_{1-x}Ca_xMnO_3$ series. Note the systematic energy shift and the enhancement of the pre-edge feature at $E \sim 6542$ eV with increased doping.

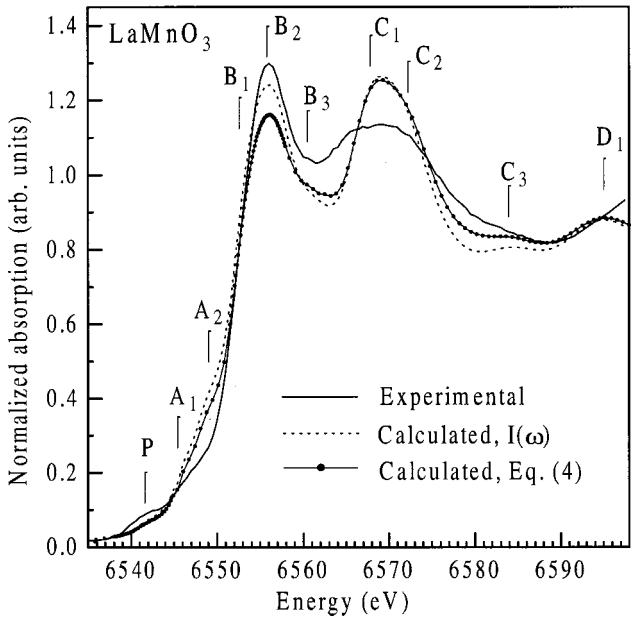

FIG. 2. A comparison of the Mn *K* edges of $LaMnO_3$. The solid line corresponds to the experimental spectrum at 300 K; dashed line shows the result of single-electron MS calculations for the 87-atom cluster; thin solid line with closed circles represents the convolution of the single-electron spectrum with the excitation spectrum shown in Fig. 7(b) below. Applying Eq. (4) gives rise to the shake-up peak B_3, lowers the intensities of the A_1 and A_2 features, and improves the agreement in the extended area $E=6575$ eV. Notice that the Hamiltonian's parameters are taken from Ref. 22 ''as they are.'' Further adjustment of these parameters is expected to bring about better agreement between the calculated and experimental spectra.

range and 0.3% for the main edge. The typical error in the relative energy calibration was 0.05 eV.[29] Since the correction[34] is almost energy independent over the 6540-6600 eV range the XANES spectra were not corrected for self-absorption. Small fluorescent backgrounds were removed and spectra were normalized to unity approximately 100 eV above the absorption threshold.

The composition dependence of the normalized Mn *K*-edge spectra of $La_{1-x}Ca_xMnO_{3+\delta}$ ($x=0$, 0.15, 0.2, 0.3, 0.4, 0.5, 0.67, and 1.0) is shown in Fig. 1. As clearly seen from the plot there is a systematic energy shift of the absorption edges with doping in good agreement with previous work.[12,27–30]

III. LOCAL STRUCTURE

To study the lattice effect in the manganites we have performed single electron calculations of the Mn *K* edge in $La_{1-x}Ca_xMnO_3$ ($x=0,0.3$) considering the structure as the origin of all variations in the Mn 4*p* states acting via changes of hybridization in a large cluster of atoms.

We shall start from $LaMnO_3$. The muffin-tin (MT) potentials were constructed for a cluster of 142 atoms assembled using the diffraction results.[35] The x-ray absorption cross sections were calculated in the dipole approximation for a cluster of 87 atoms with a basis of *s*, *p*, *d*, and *f* scattering states at each site. Two static limits, namely, fully relaxed $Z+1$ potential and unrelaxed Z potential approximations,[36] were considered. The fully relaxed potential brings about a rigid downward energy shift of 1 eV and slightly increases the intensity of the peaks just above the absorption threshold. A modified DLXANES code[37] carrying out a direct inversion of the scattering matrix was used.

To compare the calculated spectra with experimental ones, the former were convoluted with a Lorentz function. The broadening factor was taken as a sum of three constituents: core hole lifetime (~ 0.6 eV), instrumental resolution [~ 1 eV with the Si(111) monochromator at the Mn *K* edge of beamline X-19A at NSLS], and the energy-dependent photoelectron lifetime which was assumed to increase proportionally from zero at E_F to 1 eV at 100 eV above. Resultant Mn *K*-edge XANES of $LaMnO_3$ is plotted in Fig. 2 along with the experimental data (background subtracted). Both spectra were normalized to 1.0 at ~ 100 eV above the absorption threshold. As is clearly seen from the figure, the positions of the features labeled A_i, B_i, C_i, and D_i can be reasonably explained in terms of single-electron multiple-scattering (MS) calculations. However, the intensity of the pre-edge peak at 6542 eV is low and the B_3 feature that is approximately 7 eV above the main peak is missed. It should be noted that in the unbroadened XANES spectrum there is a weak peak near the observed B_3. Its intensity, however, is too small to contribute to B_3. We will discuss the origins of the pre-edge and the B_3 features in Secs. V A and V B.

The MS approach offers a pictorial view of the observed features that is briefly summarized below. We found that to reproduce the A_1 and A_2 shoulders it is important to include the *d* and *f* partial phase shifts, implying that these shoulders arise due to hybridization between the Mn 4*p* and La 5*d*

orbitals. B_1 and B_2 are Mn $4p$ states split by the crystal field. The main peaks arise for a cluster of seven atoms but they form completely for a cluster of 87 atoms, showing that the $4p$ wave function delocalizes over the large cluster, i.e., it has band character. The C_1 and C_2 features appear first when the MnO_6 octahedron is surrounded by eight La atoms. As with the *B* peaks, they tend to be fully developed for large clusters. Substantial differences in the calculated magnitudes compared to experimental ones may have two sources. First, the calculated C_1 and C_2 are undersplit. This is presumably due to the application of non-self-consistent field (SCF) potentials, or to some discrepancies between the model and actual local structures in $LaMnO_3$. Second, structural and thermal broadening seem to contribute to the smaller observed intensity. Finally, feature *D* is in the extended part of the spectrum where the XANES matches the EXAFS spectrum. Note the correct amplitude and phase behavior of the calculated spectrum over this area.

In order to simulate polaronic distortions across the MI transition in $La_{0.7}Ca_{0.3}MnO_3$ the XANES spectra were calculated twice: (i) assuming R-$3c$ symmetry of the cluster with a single Mn-O bond ($R=1.96$ Å), and (ii) using $Pbnm$ symmetry of the cluster with three different Mn-O bonds ($R_1=1.91$, $R_2=1.97$, and $R_3=2.16$ Å). It should be mentioned that a recent EXAFS study[13] of $La_{0.75}Ca_{0.25}MnO_3$ gave supporting evidence for polaronic distortions in the metallic phase. The oxygen atomic distribution with respect to the Mn site was found to be a two-peak function: four short (~ 1.92 Å) and two long (~ 2.01 Å) bonds. In the insulator regime the system shows a three-peak distribution that has been interpreted as two different MnO_6 octahedra. Nevertheless, we still lack information about how these different octahedra are matched in real space so we cannot build up a large cluster for the MS calculations. Consequently, the approximation chosen for cluster construction is not unique, although it involves qualitative changes in the Mn-O bond length distribution.

Figure 3(a) shows two experimental Mn *K*-edge spectra of $La_{0.7}Ca_{0.3}MnO_3$ taken below and above the transition temperature. We find an energy shift ~ 0.2 eV as the temperature increases from 30 to 260 K that is indicative of changes in the electronic and atomic structures. Calculated spectra are given in Fig. 3(b). As revealed in the figure the shape of the Mn *K*-edge XANES depends dramatically on the local oxygen atomic distribution. In the metallic phase the edge is sharper than in the insulator phase. Thus, the MS calculations qualitatively reproduce the observed energy shift, which, however, would be better interpreted as spectral intensity redistribution upon distortion rather than as a rigid energy shift.

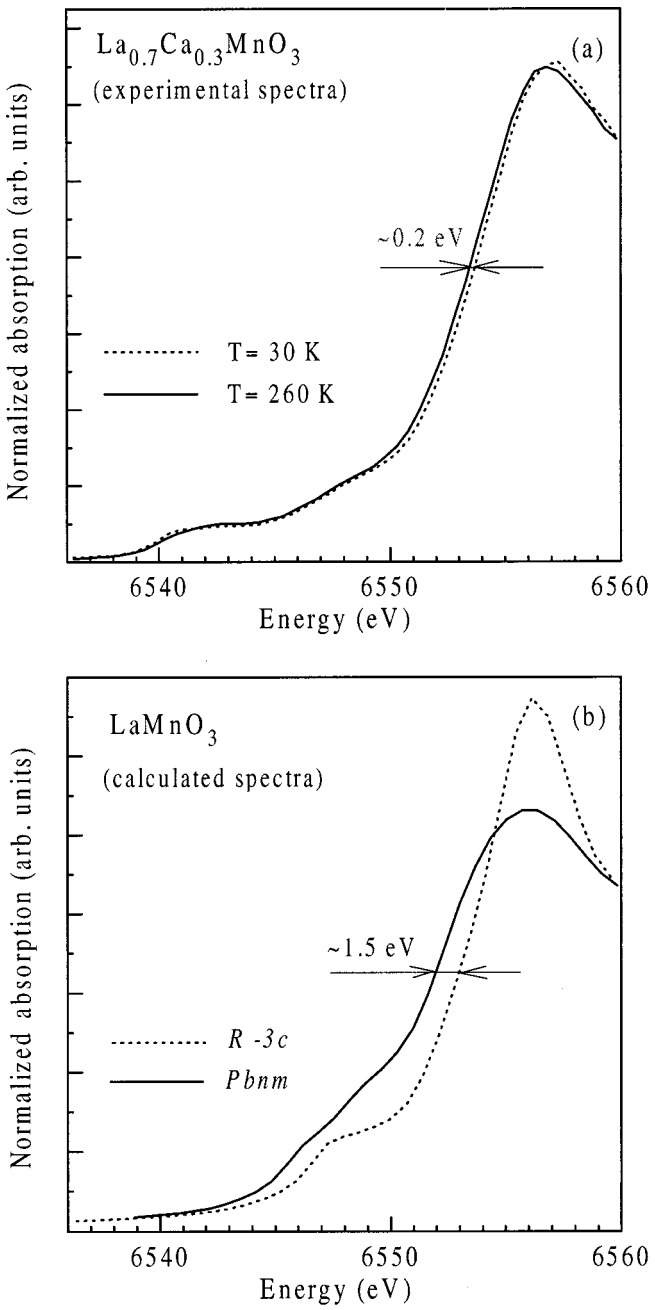

FIG. 3. (a) Normalized Mn *K* edges of $La_{0.7}Ca_{0.3}MnO_3$ measured at 30 K (dashed line) and 260 K (solid line). (b) Calculated XANES spectra showing the profound effect of local atomic distortions on the shape of the edge: fully developed (removed) distortions are simulated assuming orthorhombic (rhombohedral) structure. For both panels note the redistribution of the spectral weight from the sharper main peak to the low energies that appears as the energy shifts at the half height of the edges.

IV. MAGNETIC ORDERING

Since we intend to explore the effect of magnetic ordering on the Mn *K*-edge spectra rather than to refine the local magnetic structure of $La_{1-x}Ca_xMnO_3$ we will start from the fairly well known magnetic structures of $x=0$, 0.3, and 1. Below the Néel temperature, the stoichiometric $LaMnO_3$ is an antiferromagnetic insulator of *A* type with ferromagnetic coupling in the layers and antiferromagnetic coupling between the layers.[2] Pure $CaMnO_3$ is antiferromagnetic of *G* type where each Mn magnetic moment is orientated antiparrallel with respect to its nearest Mn neighbor.[2] $La_{0.7}Ca_{0.3}MnO_3$ exhibits a ferromagnetic-to-paramagnetic transition on warming to the Curie temperature T_c. The absolute value of the magnetic moment can be taken from ei-

ther the results of Rietveld refinement of the neutron diffraction data, or dc magnetization measurements by extrapolating the saturated magnetization to zero field.

Below we describe a procedure for a spin-dependent MT potential construction that allows one to match the calculated magnetic moment to the measured one. For simplicity, we will make some reasonable approximations, which have been widely used in x-ray magnetic circular dichroism calculations.[38] We will preserve a spherical symmetry of the atomic potentials and will ignore the exchange splitting of the core levels,[39] assuming that the local magnetic moment at the Mn sites is due to partially filled $3d$ orbitals. Furthermore, we will neglect the spin-orbit interaction of the photoelectron, which is usually an order of magnitude weaker than the exchange interaction of the photoelectron with spin-up and spin-down densities of states. In what follows the only source of spin-polarized XANES is the exchange interaction of the photoelectron with spin-up ($\uparrow$) and spin-down ($\downarrow$) densities of states.

Magnetic moment matching may be conventionally divided into the following steps. (i) Split the relativistic atomic charge density at the Mn site into spin-up and spin-down densities. (ii) Construct new overlapped charge densities around each atomic site using the Mattheiss prescription. Set $\rho_\uparrow = \rho_\downarrow = 0.5\rho$ for all sites except the Mn one. Construct the spin-dependent MT potential using the von Barth–Hedin local density approximation (LDA) exchange-correlation potential:[40] $V_{ex}^{BH} = V(\rho, x)$. (iii) Find the d-like partial DOS, and then calculate the magnetic moment at the Mn site. (iv) Compare the calculated magnetic moment with that available from neutron diffraction and dc magnetization measurements. To close the loop, one needs to repeat steps from (i) to (iv) assuming x as a varying parameter until a reasonable agreement between the calculated and experimental magnetic moments is achieved. Note that this is not a self-consistent approach; we just adjust the strength of the Mn $3d$ band splitting in order to get reasonable agreement for the local magnetic moment.

In this paper we will restrict ourselves to solving the standard nonrelativistic Schrödinger equation with spin-up and spin-down scattering potentials rather than solving the Dirac equation. The relativistic correction was found to be important for elements with large atomic number Z,[41] while we calculate spin-polarized XANES for the Mn ($Z=25$) K edge. In addition, it is not the relativistic correction but the lack of a self-consistent field cluster potential that is the leading factor limiting the accuracy of our MS calculations. We would like to point out that both relativistic and SCF potential corrections have been included in a powerful AB INITIO FEFF-8 code that has become available recently.[42] As we shell see from the next section, in complex $La_{1-x}Ca_xMnO_3$ the Mn $3d$–O $2p$ hybridization seems to have a stronger impact on the shape of the Mn K-edge spectra than does local magnetic ordering.

Figure 4 shows the spin-polarized partial density of states (PDOS) of d type for $LaMnO_3$ and $CaMnO_3$. The energy positions of the peaks agree reasonably well with results of self-consistent LDA calculations.[43] Both compounds show a clear tendency to open the gap at E_F. It is interesting to compare the observed pre-edge structure at $E \sim 6542$ eV, which is usually associated with empty Mn $3d$ states, with the calculated Mn $3d$ PDOS.

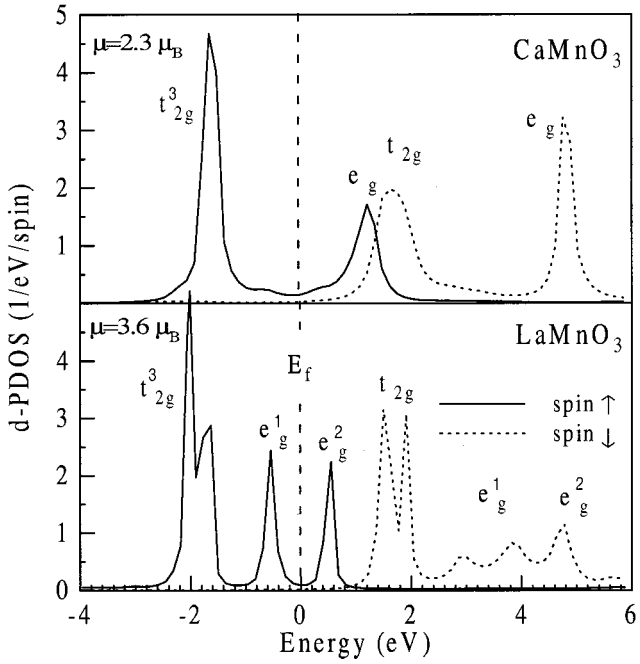

FIG. 4. Spin-polarized d-like PDOS of the orthorhombic $LaMnO_3$ and $CaMnO_3$ for 87- and 85-atom clusters as calculated applying the local magnetic moment matching approach developed in Sec. IV. Local magnetic moments on the Mn sites of $LaMnO_3$ and $CaMnO_3$ are, respectively, $\sim 3.6\mu_B$ and $2.3\mu_B$ in accordance with neutron-diffraction results (Ref. 2). The vertical dashed line represents the estimated Fermi level. Notice a tendency towards opening of the band gaps in both compounds.

As will be shown in the inset of Fig. 6, two features labeled P_1 and P_2 clearly distinguished in $LaMnO_3$ appear to correspond to the e_g^2 minority- and t_{2g} minority-spin states, respectively. The calculated energy split of 1.5 eV is somewhat smaller than the ~ 2 eV value observed experimentally. The peak that could appear from the e_g^1 and e_g^2 minority-spin states is not observed experimentally. It seems to be obscured by the more intense A_1 and A_2 features ~ 7 eV above the absorption threshold. Pre-edge structure in $CaMnO_3$ exhibits a relatively weak shoulder P_1, main peak P_2, and small feature P_3 that we tentatively assign to e_g majority-, t_{2g} minority-, and e_g minority-spin peaks in the Mn $3d$ PDOS. Calculations qualitatively predict an upward energy shift of the P_1 shoulder relative to that in $LaMnO_3$. They also give smaller P_1-P_2 splitting in $CaMnO_3$ in accordance with experimental observations. However, the accurate position of the P_2 peak is missed. These interpretations are in line with the assignment of Bridges *et al.*[28] guided by recent local spin density approximation (LSDA) + U calculations of $LaMnO_3$,[44] indicating that our simplified PDOS calculations have captured the essential details of the spin-polarized electronic structure in $La_{1-x}Ca_xMnO_3$.

Ensured that we can describe the major source of magnetic ordering in CMR compounds reasonably well, we have performed spin-polarized Mn K-edge calculations for $x=0$,

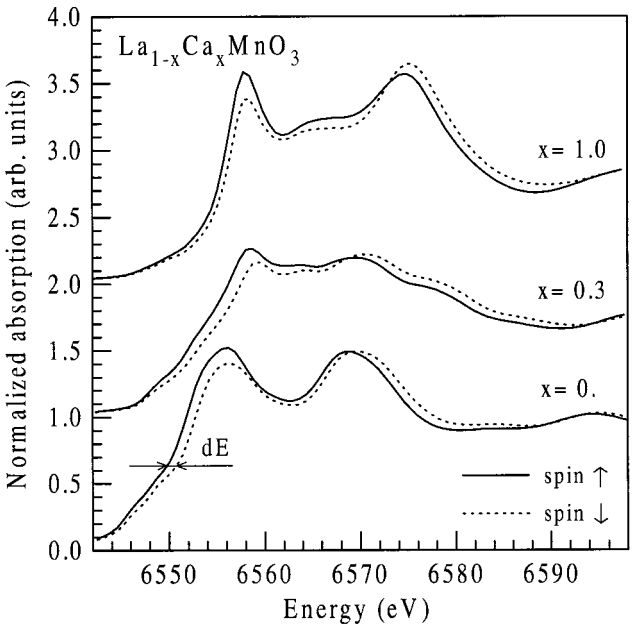

FIG. 5. The theoretical spin-polarized Mn *K* edges for $x=0,0.3,1$ after broadening. Spectra of the $x=0.3$ and $x=1$ samples are offset by 1 and 2 for clarity. The energy shift at the half height of the edge reaches a maximum of 1.1 eV in the metallic $x=0.3$ sample. Shifts of ~ 0.9 and ~ 0.5 eV are found in $LaMnO_3$ and $CaMnO_3$ roughly following the magnitude of the local magnetic moments observed on the Mn sites.

0.3, and 1. There are energy shifts between the spin-up and spin-down spectra for all compounds originating from the spin-dependent scattering of the photoelectron in the final states. Spin-up and spin-down photoelectrons experience different scattering potentials because of different Mn 3*d* spin densities. This leads to some difference in the partial phase shifts with the largest impact on resonant *d*-type scattering. The atomic like $1s \rightarrow 4p$ dipole matrix element is also spin dependent. The spin-up atomic cross section is shifted toward lower energy providing a larger relative intensity for low-energy peaks in the spin-up XANES.

The resulting spectra are shown in Fig. 5. Direct experimental observation of spin-up and spin-down XANES of CMR materials is a very sophisticated experiment that has not been reported yet. Since the conventional Mn *K*-edge spectrum is given by a sum of spin-up and spin-down spectra, $I_{\mathrm{XANES}}(E)=0.5[I_{\mathrm{XANES}\uparrow}(E)+I_{\mathrm{XANES}\downarrow}(E)]$ the splitting for spin-up and spin-down XANES spectra will contribute to the broadening. In metallic $La_{1-x}Ca_xMnO_3$ $(0.15<x<0.4)$, the resultant XANES spectrum should become narrower when crossing T_c on warming. Changes in the broadening can be monitored qualitatively, looking for the difference between two conventional XANES spectra as a function of temperature.

Comparing the calculated spin-polarized spectra with available data we can mention the following. (i) The major features of the absorption edges are well reproduced in our single-electron spin-polarized MS calculations. As in the case of the non-spin-polarized calculations, the pre-edge peaks show insufficient intensities and the B_3 features are missed. (ii) The energy shift of ~ 5 eV between the major peaks of $LaMnO_3$ and $CaMnO_3$ is in accord with the shift in the absorption edge position reported in Refs. 12, 27 and 29. Therefore, the chemical shift can be satisfactorily explained in terms of the single-electron calculations. (iii) The calculated absorption edge for the $x=0.3$ ferromagnetic sample is shifted toward higher energy by ~ 3 eV compared to the experimental spectrum. We could not reproduce the energy gap in the paramagnetic $x=0.3$ sample. This is in spite of the fact that the calculations were carried out for a heavily distorted orthorhombic structure, implying three different Mn-O bonds. Part of the discrepancy could be due to the use of non-SCF potentials, but most likely it reflects an essential limitation of the single-electron approach in the vicinity of the Fermi energy. We are unaware of SCF LDA calculations of doped manganites that would clear up the question of whether or not the onset of the structural distortions above T_c is sufficient to open the energy gap of ~ 1.5 eV as observed in the optical conductivity measurements.[45] X-ray photoemission spectroscopy (XPS) and soft x-ray absorption spectroscopy (XAS) data suggest a covalent nature of the Mn-O bond in $La_{1-x}Sr_xMnO_3$ (Refs. 18 and 20) and $La_{1-x}Ca_xMnO_3$.[19] Saitoh *et al.*[22] have reported that both $LaMnO_3$ and $SrMnO_3$ should be considered as charge-transfer type compounds (like Cu and Ni oxides). For both compounds the Mn $3d$-$3d$ Coulomb repulsion U_d is larger than the ligand *p* to Mn $3d$ charge-transfer energy Δ, which in combination with the small p-$3d$ hop integral results in opening the energy gap.[21] We will consider the effect of Mn $3d$–O $2p$ hybridization, implying that a many-body description of electronic structure is relevant to the Mn *K*-edge XANES, in the next section.

V. Mn $3d$–O $2p$ HYBRIDIZATION

One important aspect of CMR perovskites that, however, was not sufficiently discussed in previous Mn *K*-edge research, is the essentially covalent character of the Mn-O bonds, as in the Cu-based high-temperature superconductors (HTSC's). O *K*-edge measurements show that Ca doping introduces holes and these holes are primarily on the O $2p$ rather than on the Mn $3d$ orbitals.[18–20] How do the holes affect the shape of the Mn *K* edge? We can point out two features of the absorption edge shown in Fig. 2 that are related to the Mn $3d$–O $2p$ hybridization: (i) a pre-edge peak at $E\sim 6542$ eV and (ii) the feature B_3 that is $E\sim 6$ eV above the absorption maximum.

A. Pre-edge feature

The pre-edge region extends from approximately 6537 to 6552 eV. It is associated with both the dipole transitions from the $1s$ to unoccupied states having *p* symmetry with respect to the Mn absorption site and with the direct quadrupole transition from $1s$ to the empty Mn $3d$ states. The dipole transition occurs if there is a nonzero *p*-like partial density of states at the absorption site produced either through the linear combination of neighboring O $2p$ orbitals due to the breaking of the inversion symmetry at the absorption

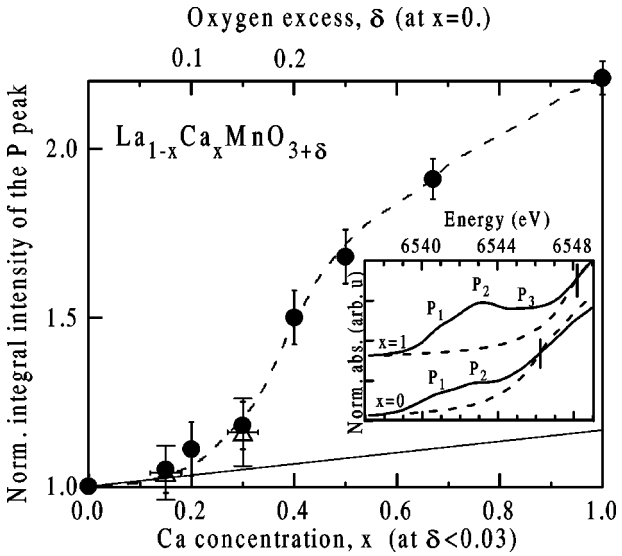

FIG. 6. The integrated intensity of the pre-edge feature as a function of Ca concentration (closed circles) in the $La_{1-x}Ca_xMnO_3$ series and oxygen excess in $LaMnO_{3+\delta}$ ($\delta=0.07,0.15$) (triangles). The solid line corresponds to the merely rigid-doping enhancement of the total Mn $3d$ spectral weight as ionic Mn $3d^4$ (with six holes on the $3d$) is converted to Mn $3d^3$ (with seven holes on the $3d$) upon Ca doping. The evolution of the Mn *K*-edge pre-edge feature with increasing x in $La_{1-x}Ca_xMnO_3$ ($x=0,0.3,1$) is shown in the inset. Dashed lines represent the $1s\rightarrow 4p$ background calculated for a restricted basis neglecting the Mn $3d$ phase shift at all Mn sites in the 87-atom cluster except for the absorbing atom (Mn $4p$ and Mn $3d$ hybridization excluded). Vertical bars show the upper limits used to evaluate the integrated pre-edge intensity.

site[46] or through the linear combination of the Mn $3d$ orbitals centered at neighboring Mn ions.[44] In order to give a correct interpretation of the pre-edge feature one needs to know which channel dominates. A raw estimate for the strength of the two channels is possible if one takes advantage of recent LSDA+U calculations by Elfimov *et al.*[44] The broadened (due to the core hole lifetime) density of states in $LaMnO_3$ shown in Fig. 2 of Ref. 44 reveals the roughly correct proportion between the intensities in the pre-edge features and in the main peak. Bearing in mind that the dipole matrix element is a smooth function of energy that could not alter the previous result we concluded that the dipole channel dominates in the pre-edge peak.

The integrated intensity of the pre-edge feature was normalized to the value for the stoichiometric $LaMnO_3$ sample and plotted against (x,δ) in Fig. 6. Within the error bars, the oxygen deficiency brings about the same number of holes as does $x=2\delta$. Oxygen-deficient samples have a smoother shape for the pre-edge peaks, indicating apparently larger structural distortions than in those stoichiometric oxygen samples with $x=2\delta$. Further EXAFS determinations will be needed to verify this assignment. As is evident from Fig. 6, the integral spectral weight increases faster than is expected for rigid doping of Mn $3d$. To explaine this, any changes in electronic and local structure must have a much stronger impact on the narrow bands (such as Mn $3d$ and O $2p$) than on the broad (Mn $4s$ or Mn $4p$) bands. Therefore, it is the Mn $3d$ and O $2p$ hybridization (forming the valence and conduction bands in the CMR materials) that is expected to exhibit the strongest variations. The energy dependence in the pre-edge region is controlled through unoccupied Mn $3d$ and O $2p$ states, while the intensity in this region is affected both by the unoccupied density of states and by hybridization between the Mn $3d$ and Mn $4p$ states on neighboring atoms. The former implies that the pre-edge feature inherits the energy dependence of the unoccupied band and, to a first approximation, the Mn $3d$ PDOS can be used to classify the peaks at the pre-edge (Sec. IV). The hybridization is expected to be strongly enhanced as the mean Mn-Mn distance decreases with increased doping. This is exactly what is seen in Fig. 6, where at least 100% incease in the intensity occurs due to the enhancement of Mn $3d$ and Mn $4p$ hybridization. For this reason it is impossible to associate the changes in the integrated pre-edge intensity with variations in the total Mn $3d$ PDOS from the x dependence. In contrast, if the Mn $3d$ and Mn $4p$ hybridization does not change, the measured integral intensity should be directly proportional to the total Mn $3d$ PDOS. Temperature-dependent variations in $La_{1-x}Ca_xMnO_3$ could be satisfactory examples of those changes. We will consider the temperature dependence of the pre-edge region for $x=0.3$ and $x=0.67$ samples in Sec. VI B.

B. Shake-up transition

It is well known that the ground state of $LaMnO_3$ can be described as a linear combination of the many-body electronic configurations $\gamma|3d^4\rangle+\beta|3d^5L\rangle+\gamma|3d^6L^2\rangle$.[22,47,48] The appearance of the Mn $1s$ core hole due to the $1s\rightarrow 4p$ transition results in strong perturbations in the many-body system. For instance, the $3d^4$ configuration exhibits an upward energy shift because of $1s$-$3d$ hole-hole repulsion-Q. To correctly account for the perturbations in the electronic structure upon the sudden switching on of the core hole we introduce an excitation function $S(\omega)$. Two static limits of the so-called final state rules should be considered. In the unrelaxed Z approximation the N-hole final state is affected by the Mn $1s$ core hole. The excitation spectrum $S(\omega)$ is given by the sum over all fth final N-hole states projected to the ground state N-hole wave function without the core hole:

$$S(\omega)=\sum_f |\langle\Psi_f(N)|\Psi_0(N)\rangle|^2\delta(\omega-E_f(N)+E_0(N)). \tag{1}$$

In the fully relaxed $Z+1$ approximation, the Mn atom is replaced by Fe, which adds one electron to the absorption site creating the $(N-1)$-hole final state with the Mn $1s$ core hole:

$$S(\omega)=\sum_f |\langle\Psi_f(N-1)|c_{i,\sigma}|\Psi_0(N)\rangle|^2\delta(\omega-E_f(N-1)+E_0(N)). \tag{2}$$

In Eqs. (1) and (2) Ψ_0 is the ground state with energy E_0 and Ψ_f is the fth excited state with energy E_f referred to Hamil-

tonians in the initial, H_0, and final, H_f, states, respectively. In the case of CMR compounds, the Hamiltonian is not well established yet. It might be taken as a combination of the Anderson-Hasegawa Hamiltonian[6] with the O $2p$ to Mn t_{2g} hole exchange interaction added and the Peierls-Hubbard[49] Hamiltonian, containing essential physics compatible with experimental observations of magnetization and transport properties,[16] low-temperature optical,[45] photoemission,[22] O *K*-edge XAS,[19,20] electron-energy-loss spectroscopy,[18] and local structure measurements.[12,13] Here we present a simplified calculation for the low-spin system ignoring the charge-lattice and spin-lattice couplings but retaining the proper description for covalent Mn-O bonds. The electronic structure will be treated in the framework of the Hubbard Hamiltonian,

$$H_0=\sum_{i,\sigma}\epsilon_i n_{i,\sigma}+U_d\sum_i n_{i,\uparrow}n_{i,\downarrow}+\sum_{k,\sigma}\epsilon_k n_{k,\sigma}+U_p\sum_i n_{k,\uparrow}n_{k,\downarrow}+V_{dp}\sum_{\langle i,k\rangle\sigma,\sigma'} n_{i,\sigma}n_{k,\sigma'}+V_{pp}\sum_{\langle k\neq k'\rangle\sigma,\sigma'} n_{k,\sigma}n_{k',\sigma'}-T_{dp}\sum_{\langle i\neq k\rangle\sigma,\sigma'}(c^\dagger_{i,\sigma}p_{k,\sigma'}+\text{H.c.})-T_{pp}\sum_{\langle k\neq k'\rangle\sigma,\sigma'}(p^\dagger_{k,\sigma}p_{k',\sigma'}+\text{H.c.}) \quad (3)$$

where c creates a hole with spin σ at site i (k) in the Mn $3d$ (O $2p_\parallel$) orbitals, respectively; $n_{i,\sigma}=c^\dagger_{i,\sigma}c_{i,\sigma}$ and $n_{k,\sigma}=p^\dagger_{k,\sigma}p_{k,\sigma}$ and are hole number operators; ϵ_i and ϵ_k are Mn $3d$ e_g and O $2p_\parallel$ energies; U_d and U_p are Mn and O on-site Coulomb repulsions; V_{dp} and V_{pp} are off-site Mn-O and O-O Coulomb repulsions; and T_{dp} and T_{pp} are the Mn-O and O-O nearest-neighbor hops. The specific point of the Hamiltonian (3) is the introduction of the O $2p$ band which we believe will better account for the charge transfer in CMR compounds. In the final states $H_f=H_0+H_c$, where H_c is subject to the $1s$-$3d$ interhole Coulomb repulsion Q.

The final state rule[36] has been developed from model calculations of the dynamic response of the conduction electrons to the suddenly switched on core hole potential. These model calculations may be applicable directly to simple metals, but in more complex systems the final state rules probably need to be systematically tested. Such tests are beyond the scope of the present paper. We will employ the Z approximation to illustrate several important aspects of $S(\omega)$ behavior as a function of the Hamiltonian parameters. Whatever the approximations, the *K*-edge XANES spectrum can be obtained as a convolution product of the single-electron transition from the $1s$ core level to the unoccupied electronics states $I(\omega)$ and the $S(\omega)$,[50]

$$\sigma(\epsilon)=\int S(\omega)I(\omega-\epsilon)d\epsilon, \quad (4)$$

which is valid as long as the interaction between N-hole states and the $4p$ photoelectron can be neglected. $I(\omega)$ was calculated for the cluster of 87 atoms as described in Sec. III.

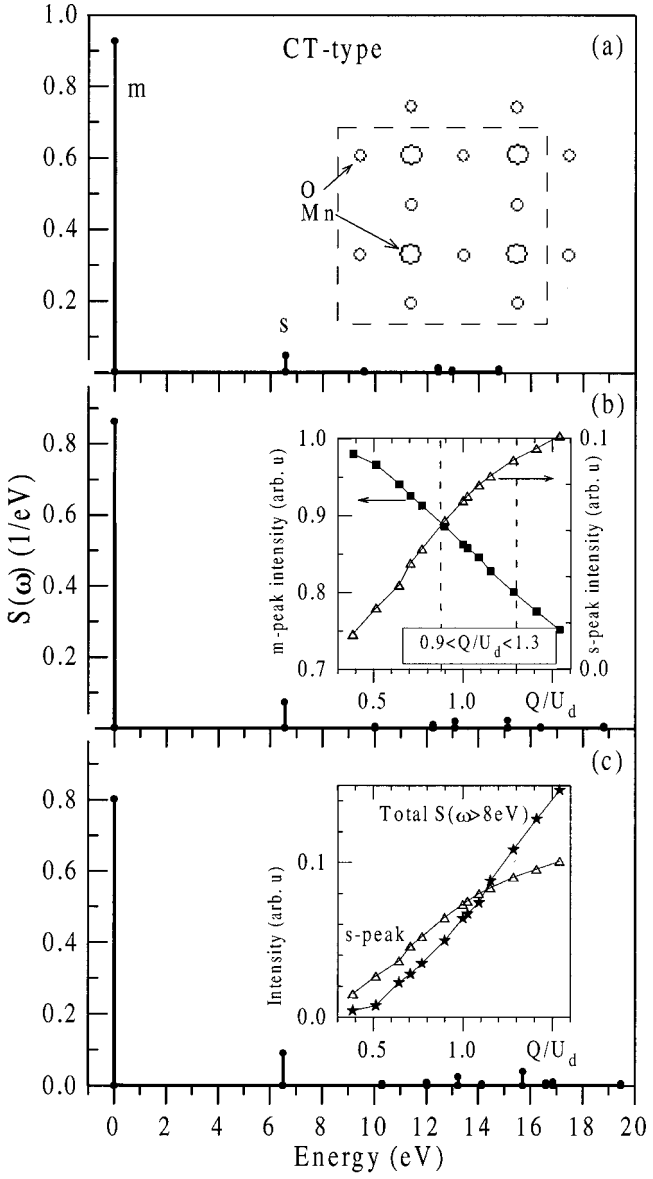

FIG. 7. The excitation spectra of $LaMnO_3$ as a function of Mn $1s$-$3d$ Coulomb repulsion: (a) $Q=5$, (b) $Q=7.8$, and (c) $Q=10$ eV. The excitation spectra are calculated in the Z approximation for a four-hole wave function in a 12-atom cluster, Mn_4O_8, shown in the inset of (a). $U_d=7.8$, $\Delta=4.5$, and $(pd\sigma)=-1.8$ eV are taken from Ref. 22. Spectral weights of the main peak (m), first satellite (s), and other peaks altogether vs Q are plotted in the insets of (b) and (c).

The Lanczos technique was employed for numerical diagonalization and spectral calculation of $S(\omega)$ in a two-dimensional cluster of 12 atoms. The cluster consisting of four Mn and eight O atoms with periodic boundary conditions is shown in the inset of Fig. 7(a). The total number of holes for $LaMnO_3$ is 4. One more question to be addressed before discussing the results of our computation is that of static versus dynamic valence fluctuations. In the framework of exact diagonalization one deals with the stationary Hamiltonian (3). That means that the dynamic effects are averaged and spread over a cluster of finite size, so they appear as

static effects. Actually, it is not so bad an approximation as it may appear at first. A fast XANES picture of the local valence state (slower than 10^{-14} s) has to be averaged over all possible space realizations, since the Mn *K*-edge XANES is a bulk-sensitive technique. If the ergodic hypothesis is true on local length scales and the average over space is equal to the average over time then XANES is not sensitive to the static versus dynamic valence fluctuations. This justifies applying the stationary Hamiltonian to our analyses.

For simplicity we retain only three parameters in the Hamiltonian: U_d, Δ, and T_{dp}. Saitoh *et al.*[22] have analyzed Mn $2p$ XPS spectra using the cluster model. From the fit to the experimental data they found $U_d=7.8$, $\Delta=4.5$, and the p-d transfer integral $(pd\sigma)=-1.8$ eV $[T_{dp}=3|(pd\sigma)|]$. The energy gap is the difference between the first electron addition and removal states, $E_g=E(N+1)+E(N-1)-2E(N)$. For a four-hole wave function in the Mn_4O_8 cluster, $E_g\sim 1.6$ eV. The hole occupation numbers are found to be 0.62 and 0.19 at the Mn and O sites, respectively. This implies an electron occupation number on the Mn site of 4.36, i.e., larger than the nominal 4.0 value expected for an ionic Mn $3d^4$ configuration.

We treat the repulsion between the Mn $1s$ core hole and $2d$ holes as a local Coulomb potential Q on the absorbing site. For Mn $2p$ XPS simulations the Coulomb repulsion is usually 30% larger than U_d.[47] Since the $1s$ core is screened by the closed $2p$ shell the $1s$-$3d$ repulsion should be smaller than the $2p$-$3d$ one. Consequently, $Q=1.3U_d$ may be viewed as an upper limit in our computation. Figures 7(a–c) show the excitation spectra calculated for $Q=5$, 7.8, and 10 eV, respectively. For a four-hole wave function in the 12-site cluster with $S_z=0$ the total number of peaks is 4356. However, only a few of them contribute to $S(\omega)$. The major peak and the satellite, marked as *m* and *s* in Fig. 7(a), are due to the $1s^1\cdots 3d^4 4p^1$ and $1s^1\cdots 3d^5 L 4p^1$ final states reached in x-ray absorption. The position of the *s* peak is almost Q independent because the holes pushed from the absorption site are redistributed over other atoms in the 12-site cluster. By means of direct simulation, using Eq. (4) we made sure that in order to be distinguished as the shake-up peak [at a level of broadening in $I(\omega)$ of ~ 2 eV] the *s* peak in $S(\omega)$ must have at least 6% (0.06 eV^{-1}) spectral intensity. The inset of Fig. 7(b) shows the intensities of the *m* and *s* peaks vs Q/U_d, from which one finds $Q\sim 0.9U_d$ as a low limit for the $1s$-$3d$ repulsion that would yet provide sufficient magnitude for the shake-up peak. The total intensity of higher-energy satellites ($\omega>8$ eV) increases rapidly with Q and at $Q\sim 1.1U_d$ it exceeds the intensity of the *s* peak as shown in the inset of Fig. 7(c). For the specified set of Hamiltonian parameters the two-shell absorption based on the simple cluster model[51] is no longer valid because of the limitation of its basis.

The resultant Mn *K*-edge XANES spectrum, calculated as the convolution product of the single-electron absorption and many-body excitations, is plotted in Fig. 2 along with the purely single-electron and the experimental spectra. The inclusion of the excitation spectrum (i) introduces the additional broadening, (ii) rescales the absolute energy, and (iii) improves the overall agreement. In particular, the shake-up peak B_3 appears.

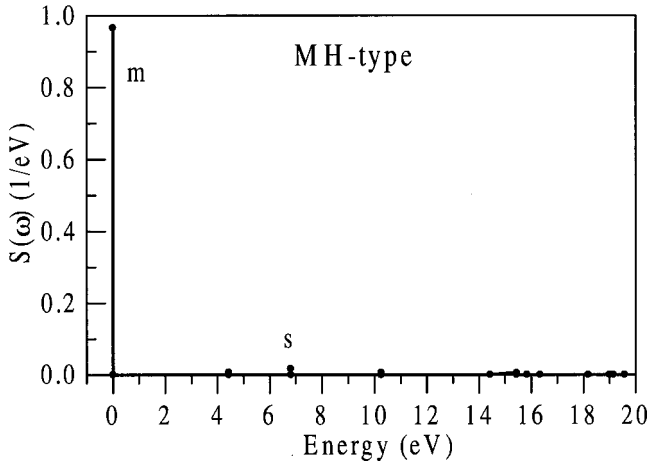

FIG. 8. The theoretical excitation spectrum of $LaMnO_3$ calculated using the U_d, Δ, and $(pd\sigma)$ from Ref. 48, implying a Mott-Hubbard-type insulator. The magnitude of the calculated satellite *s* peak is too small to substantially contribute to the shake-up peak observed experimentally. Comparing the $S(\omega)$ functions depicted in this plot with those in Fig. 7 we conclude that $LaMnO_3$ is a charge-transfer-type insulator rather than a Mott-Hubbard-type insulator.

It is worth mentioning that there is another set of U_d, Δ, and $(pd\sigma)$ parameters satisfying the Mn $2p$ XPS data on $LaMnO_3$. Chainani *et al.*[48] found $U_d=4$, $\Delta=5$, and $(pd\sigma)=-2.2$ eV, assuming that $LaMnO_3$ is a Mott-Hubbard-type compound. To verify this we have performed $S(\omega)$ calculations using the parameters of Chainani *et al.* and assuming $Q=U_d$. The excitation spectrum is shown in Fig. 8. The satellite peak arises approximately 7 eV above the main peak, in good agreement with the relative position of the B_3 with respect to the B_2 peak in the experimental Mn *K*-edge spectrum. However, the calculated intensity of the satellite peak (1.6%) lies far below the level that would provide a reasonable magnitude for the B_3 feature. In attempts to gain larger satellite intensity, Δ was allowed to vary, staying within the Mott-Hubbard (MH) regime. The estimated 6% threshold for *s*-peak spectral weight was crossed for $\Delta>11$ eV (at $Q=U_d$) and $\Delta>7$ eV (at $Q=1.3U_d$)—both values seem to be too large to be meaningful. From these results we conclude that Saitoh *et al.* parameters provide better agreement with the experimental Mn *K* edge of $LaMnO_3$. Thus, $LaMnO_3$ is in the CT-type rather than in the MH-type regime.

The shake-up peak in the Mn *K*-edge spectra of $La_{1-x}Ca_xMnO_3$ is not so distinct as, for example, in the Cu *K* edge of the $La_{2-x}Sr_xCuO_4$ superconductor. There might be three reasons for this. First, HTSC's have a strong anisotropy of the electronic and local structure in the CuO_2 planes and in the direction perpendicular to the plane. Polarized Cu *K*-edge XANES measurements with $\mathbf{E}\|ab$ (x-ray polarization vector $\mathbf{E}$ is in the CuO_2 planes) show a pronounced shake-up peak,[52] providing supporting evidence for the pre-

dominantly in-plane character of the doped holes. Although $La_{1-x}Ca_xMnO_3$ is also strongly anisotropic, the character of the doped holes seems to be three dimensional. Secondly, the CMR materials are characterized by a much more distorted local structure compared to that in the HTSC's. As shown in Secs. III and IV, both structural and spin-polarized-driven components of the broadening can reduce the contrast of the weak peaks, including the shake-up peak. Thirdly, and probably most important, the CMR materials are not such well defined CT-type compounds as the HTSC's. At approximately similar values of T_{dp}, $U_d-\Delta$ is ~ 6 and ~ 3 eV in cuprates and manganites, respectively. A stronger O $2p$ character of the doped holes in cuprates results in the more distinct shake-up peak. Apparently, the near relation of the CMR compounds to MH type (or their not well defined CT-type nature) promotes the onset of magnetic ordering in the doped compounds. Through a certain admixture of the Mn $3d^4$ to the ground state the conventional DE mechanism is allowed. This regime also gives rise to substantial exchange interaction between the O $2p$ ligand holes and the localized spins of the Mn atoms, thereby enhancing the hopping of the holes (T_{dp} and T_{pp} in the Hamiltonian) upon onset of the FM order. Since the ground state of doped manganites is mostly O $2p$–like[18–20] (CMR materials are CT type, although not well defined) the exchange between the ligand holes and the localized spins must govern the electronic properties at low temperatures. It is worth mentioning that Alexandrov and Bratkovsky[53] have recently explained the resistivity peak and the colossal magnetoresistance of doped manganites as a result of carrier density collapse that is driven by the exchange interaction of polaronic carriers with the localized spins.

VI. DISCUSSION

We must first establish the relative orders of magnitude of the effects governing the fine details of the main peaks of the Mn *K* edge considered in Secs. III–V. Below they are listed from largest to smallest dimension: (i) The covalent nature of the Mn-O bond: Expected corrections in the energy scale are about 6 eV, provided that the higher-energy excitation channels have negligible spectral weights. (ii) Local structure distortions can bring about a 1.5 eV spectral weight redistribution if one considers the transition from fully developed JT distortions to an almost undistorted rhombohedral structure in $LaMnO_3$. (iii) Local spin ordering, which seems to maximize at $x\sim 0.3$, could manifest itself as ~ 1 eV splitting of the Mn $4p$ states due to spin polarization of the Mn $3d$ band.

Local orbital ordering and charge ordering are not considered here. Local orbital ordering may be viewed as one possible type of local charge ordering. In general, the CO is coupled with local structure distortions, which presumably stabilize charge redistribution. Any ''structural'' CO would essentially interfere with the charge disproportionation emerging from the Mn $3d$–O $2p$ hybridization. A combination of at least two but most likely three ''simple'' components constituent in CO takes it beyond the scope of the present paper.

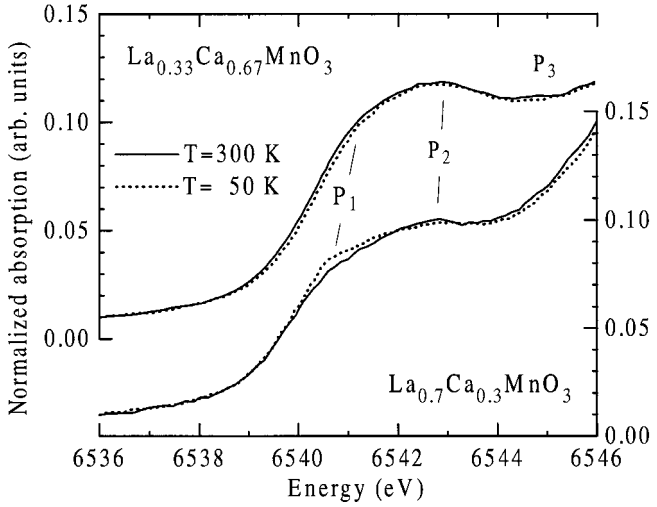

FIG. 9. Mn *K*-edge pre-edge feature of $La_{0.7}Ca_{0.3}MnO_3$ and $La_{0.33}Ca_{0.67}MnO_3$ measured at 50 K (dashed lines) and at 300 K (solid lines). Notice that the temperature dependence of the $x=0.67$ sample is almost the reversed of that of the $x=0.3$ sample.

A. Temperature dependence of the Mn *K* edge of $x=0.3$ and $x=0.67$

The Mn *K* edge can be conventionally divided into the pre-edge (Sec. V A) and the main edge. We shall start from the former. Figure 9 shows the temperature dependencies of the Mn *K* edge of $La_{0.7}Ca_{0.3}MnO_3$ and $La_{0.33}Ca_{0.67}MnO_3$. The trend of the thermal changes both of the pre-edge and of the main edge (not shown) for the $x=0.67$ sample is reversed from that observed for the $x=0.3$ sample, although the former sample shows a weaker temperature dependence. Spectral transfer from high to low energy in the $x=0.3$ sample at $T<T_c$ is in qualitative agreement with the results of optical absorption measurements for the $La_{1-x}Sr_xMnO_3$ ($x=0.175$) metallic sample[45] which exhibits a gradual filling of the pseudogap as the temperature decreases. These results along with the temperature-dependent resonance photoemission spectroscopy (RPES) of $La_{0.67}Ca_{0.33}MnO_3$ provide supporting evidence for the narrowing of the charge-transfer gap (maybe a pseudogap) below T_c. A similar trend is clearly seen for the temperature dependence of the low-energy empty states in the $x=0.67$ sample. P_1 is pulled down above T_{CO} which would reduce the gap. RPES data will be needed to make an accurate assignment.

A slight increase in the average Mn valence for $x=0.5$ and $x=0.67$ at low temperature has been put forward recently[30] to explain the temperature dependence of these edges. As revealed from Fig. 9, the integrated intensity of the pre-edge peak appears to decrease when *T* moves from 50 to 300 K. Similar tends are clearly seen for the $x=0.5$, 0.67 spectra in Ref. 30. A visible reduction of the intensity in the P_1-feature region, with little change at the P_2 and P_3 peaks, indicates a lowering of the unoccupied density of states below T_{CO}. A smaller fraction of unoccupied states means a smaller Mn $3d$ hole density, and, therefore, the formal Mn valence seems to go down at low temperatures. As we shall discuss in Sec. VI B, that is consistent with predominant hole ordering on the O $2p$ rather than on the Mn $3d$ orbital.

Next, we shall consider the temperature dependence of the main edge ($E \sim 6546$–6580 eV). The main-peak structure of the $x=0.3$ sample gets broader. As we have discussed in Sec. IV, ferromagnetic ordering brings about its own mechanism for the broadening, which, however, appears to be weaker than the structural broadening considered in Sec. III. As for the $x=0.67$ sample, within the accuracy of our measurements the spectrum collected at 300 K is as broad as that collected at 50 K. Generally, XANES spectra become broader as temperature increases because of thermal motion. It is also remarkable that the stoichiometric $LaMnO_3$, which has substantial static broadening associated with the JT distortions of the MnO_6 octahedra, exhibits a smaller broadening than the $La_{0.33}Ca_{0.67}MnO_3$ sample as temperature increases from 50 to 300 K. We speculate that such an unusual temperature dependence might be understood by assuming a partial reduction of the local distortions above T_{CO}. Although detailed local structure is unavailable yet, the diffraction data capturing an averaged picture of the local distortions do support a partial reduction of the distortions above T_{CO} for $x=0.5$ (Ref. 4) and $x=0.67$ (Ref. 33) samples. Further experimental probes of the local structure of $x=0.67$ sample are clearly motivated by this work. The onset of the weak ferromagnetic interaction could contribute to the total broadening above T_{CO}. However, magnetization measurements imply a very small variation across T_{CO}, so we do not expect substantial changes in the spin-up and spin-down scattering potentials. As a consequence, the total XANES (taken as a sum of spin-up and spin-down spectra) will be almost unchanged. Our estimates show that structural variations of 0.1 Å affect the Mn K edge to a larger extent than magnetization variation does.

For $x=0.3$ and 0.67 the changes in the total Mn $3d$ spectral weight estimated from Fig. 9 are relatively small. Consequently, to the first approximation, a minor variation in the excitation spectrum will have a small impact on the shape of the Mn K edge as prescribed by Eq. (4).

To summarize the observed temperature dependencies of the main edge in the $x=0.3$ and 0.67 samples, we have considered three mechanisms governing the shape of the XANES spectra and found that the lattice effect is most likely to dominate in the temperature dependencies across T_c and T_{CO}.

B. Charge ordering in $La_{0.33}Ca_{0.67}MnO_3$

Qian *et al.*[30] have argued for a slight increase in the average Mn valence in the $x=0.5$ and 0.67 compounds at low temperatures, which implies an increase in the unoccupied Mn $3d$ states (i.e., larger hole density at Mn $3d$). However, the onset of the charge ordering state is not necessarily accompanied by charge ordering in the Mn $3d$ states. Because of the covalent nature of the Mn-O bond the holes are spread between the Mn $3d$ and O $2p$ states and the charge ordering at the oxygen sites is another possibility to consider.

The hole occupation number on the Mn site appears to be in a delicate balance with hole occupation number(s) on the oxygen site(s). At the level of doping x, the next Δx holes added are distributed between the Mn $3d$ and O $2p$ orbitals: $\Delta x = C_1(x) + C_2(x)$. Since $U_d > \Delta$ then $C_2 > C_1$ at a low level of doping. As the holes keep filling the O $2p$ orbitals, they often encounter one another. Oxygen on-site (U_p) and oxygen-oxygen nearest-neighbor (V_{pp}) Coulomb repulsions become players in the energy balance governing the charge distribution. C_1 will grow faster at the expense of C_2; nevertheless, the presence of the oxygen component of the charge disproportionation seems to allow $C_2 > C_1$ over a broad range of Ca doping, possibly until $x=1$. Indeed, O K-edge measurements[19,20] provide an experimental probe of the unoccupied O $2p$ states in $La_{1-x}Ca_xMnO_3$. The spectra show a pre-edge peak at $E \sim 529$ eV just above the absorption threshold which systematically increases with increasing Ca doping in accordance with the predominant O $2p$ character of added carriers. Park *et al.*[19] found that the absorption spectrum of the doped sample could be approximated by a linear combination of the $LaMnO_3$ and $CaMnO_3$ spectra, assuming a linear dependence of the spectral features on Ca substitution. This implies a linear dependence of the pre-edge integrated intensity vs x, so that since $C_2 \sim 1$ at low x $C_1 = 1 - C_2 \sim 0$ over the whole range of doping. An independent probe of $C_1(x)$ is not easily accessible through the Mn K-edge measurements because of the strong x dependence of Mn $3d$–Mn $4p$ hybridization. However, at fixed x, the temperature dependence of the pre-edge integrated intensity is a signature of the variations in the Mn $3d$ PDOS, as we argued in Sec. VI A. Consequently, a slight decrease in the integral intensity of the pre-edge peak of $La_{0.33}Ca_{0.67}MnO_3$ as the temperature falls from 300 to 50 K shows a slight redistribution of the holes from Mn $3d$ toward O $2p$, giving supporting evidence for charge ordering at oxygen sites.

Another argument for charge ordering on the oxygen sites instead of the manganese sites comes from the type of lattice distortion observed upon the onset of CO. Ground state energies of several strongly correlated systems with lattice degrees of freedom have been evaluated numerically.[49,54,55] To gain energy, the holes introduced with doping couple either with oxygen displacing modes or with ferroelectric modes referred to the metal site via a moderate electron-phonon interaction. To the best of our knowledge, ferroelectriclike displacements of Mn atoms have not been observed experimentally. On the other hand, there are plenty of diffraction data on $x=0.5$ (Ref. 4) and $x=0.65$ (Ref. 33) compounds; indicating marked displacements of oxygen atoms below T_{CO}. Although these data differ in the magnitudes and components of oxygen atom displacements they do agree on two issues: (i) the MnO_6 octahedra get more distorted and (ii) the Mn-O distortions are mostly of the breathing type when the structures are compared at room and at helium temperatures. From these data we suggest the CO to be associated with the oxygen sites.

C. Microscopic Mn valence

Finally, we shall discuss briefly the Mn valence states in manganites. The results of spectroscopic studies[19,22] show that the ground state electronic configurations in $LaMnO_3$ and $CaMnO_3$ are not the ionic ones (Mn^{4+} and Mn^{3+}) but

$\alpha_1|3d^4\rangle+\alpha_2|3d^5L\rangle+\alpha_3|3d^6L^2\rangle$ and $\beta_1|3d^3\rangle+\beta_2|3d^4L\rangle+\beta_3|3d^5L^2\rangle$, respectively. For intermediate doped compounds we suggest the ground state to be a superposition of the end member electronic configurations with possible disproportionations of $3d^5L\rightarrow 0.5(3d^5+3d^5L^2)$ and $3d^4L\rightarrow 0.5(3d^4+3d^4L^2)$ in the *distorted lattice*.[54] In real CMR systems every many-body electronic configuration carries additional spin and site indices, showing that it is spin and local structure dependent. Mathematically, one needs to find the expansion coefficients, $\gamma_i=\gamma_i(\sigma_i,R_i)$,

$$\begin{aligned}|\Psi_0\rangle=&\gamma_1|3d^5,\sigma_1,\{R_{1i}\}\rangle+\gamma_2|3d^4,\sigma_2,\{R_{2i}\}\rangle\\&+\gamma_3|3d^5L,\sigma_3,\{R_{3i}\}\rangle+\gamma_4|3d^6L^2,\sigma_4,\{R_{4i}\}\rangle\\&+\gamma_5|3d^3,\sigma_5,\{R_{5i}\}\rangle+\gamma_6|3d^4L,\sigma_6,\{R_{6i}\}\rangle\\&+\gamma_7|3d^5L^2,\sigma_7,\{R_{7i}\}\rangle+\gamma_8|3d^4L^2,\sigma_8,\{R_{8i}\}\rangle,\end{aligned}\tag{5}$$

and minimize them with respect to spin and local displacement degrees of freedom. In the relation (5) we listed the electronic and local displaced configurations explicitly, while keeping the configuration-dependent spin indices unspecified. Note that the above formulation is equivalent to finding the ground state energy and corresponding wave function which is well known to be a complete description of a quantum mechanical system at zero temperature. Therefore, microscopic solution of the Mn valence would reveal local structural distortions and local magnetic structure.

If $|\Psi_0\rangle$ is the ground state wave function, then the microscopic Mn valence at the ith site is an occupation number: $N_{i,\sigma,\{R_i\}}=\langle\Psi_0|c^\dagger_{i,\sigma}c_{i,\sigma}|\Psi_0\rangle$, where $c^\dagger_{i,\sigma}$ ($c_{i,\sigma}$) creates (annihilates) a hole in Mn $3d$ with spin and the local Mn-O displaced configuration $\{R_i\}$. The macroscopic valence probed by conventional XANES is given by a superimposed average of the microscopic states taken over all possible local and spin configurations. Spin-polarized XANES and anomalous diffraction XANES (DANES) are expected to be able to capture the microscopic valences associated with majority-(minority-)spin orientations and specific atomic sites.[56]

A single ''intermediate'' Mn valence as suggested in Ref. 27 would mean only one δ-functional peak in the excitation spectrum Eq. (1). Subías *et al.* mentioned that Mn ions could be spread over a narrow range of energy because of different local environments in doped samples, still forming the one type of Mn detected by Mn *K*-edge XANES. Notice that the peaks in our excitation spectrum are spread over more than a 10 eV range. The separation between the main and shake-up channels ($\sim$6 eV) is larger than the observed chemical shift ($\sim$4.2 eV) as x goes from 0 to 1. The one-type-Mn valence model fails to reproduce the shake-up feature in the XANES. It assumes a structureless XPS spectrum, and gradual hole filling on Mn $3d^4$ states upon doping, both inconsistent with experimental observations.[18,20,22] Again, it seems to be difficult to reconcile a unique Mn valence with observations of the CO states for $0.5<x<0.7$,[3,4] and different types of MnO_6 octahedra across T_c (Ref. 13) or T_{CO}.[4,33] In a model assuming a mixture of Mn $3d^n$ and Mn $3d^{n+1}$ with different numbers of holes at Mn sites,[30] the Mn valence can disproportionate *locally*, consistent with local lattice distortions and local magnetic order. However, since the O $2p$ band is excluded, the average Mn valence is always prescribed by the level of doping x. Restriction of the basic Eq. (5) to a mixture of Mn $3d$ configurations

$$\begin{aligned}|\Psi_0\rangle=&\theta_1|3d^5,\sigma_1,\{R_{1i}\}\rangle+\theta_2|3d^4,\sigma_2,\{R_{2i}\}\rangle\\&+\theta_3|3d^3,\sigma_3,\{R_{3i}\}\rangle\end{aligned}\tag{6}$$

implicitly assumes a Mott-Hubbard-type material according to the Zaanen-Sawatzky-Allen classification.[21]

Our detailed analysis of the Mn *K* edge spectra along with the O *K*- and Mn $L_{3,2}$-edge results[18,20] shows that $La_{1-x}Ca_xMnO_3$ is in the charge-transfer-type regime in the range from $x=0$ at least until $x=0.67$. In the Z approximation a CT-type model shows a larger magnitude of the shake-up peak than a MH-type model, providing better agreement with the experimental data in $LaMnO_3$. The shake-up peak B_3 is also clearly seen in the Mn *K*-edge XANES of the $x=0.67$ sample. It is more interesting, however, to trace the temperature dependence of the pre-edge peak across T_{CO} as shown in Fig. 9, which is in good agreement with all previous XANES data.[28,30] Assuming the restricted basis (6) to be sufficient to discribe the ground state in CMR materials, it seems to be difficult to explain why the system undergoes a transition to a $\sim$0.1–0.2 eV higher ''ground'' state with decreasing temperature. To reconcile the onset of the CO states with the experimentally observed increase in ground state energy, we expand the basis, suggesting not $|3d^3+3d^4,\sigma_i,\{R_i\}\rangle$, but $\Sigma_k|3d^kL^m,\sigma_i,\{R_i\}\rangle$ [as in relation (5) with $k=4,5$ and $m=1,2$] to dominate in the ground state of the $La_{0.33}Ca_{0.67}MnO_3$. The $|3d^kL^m\rangle$ electronic degree of freedom seems to be lowered at $T<T_{CO}$ in order to balance the total energy. The $\Sigma_k|3d^kL^m,\sigma_i,\{R_i\}\rangle$ state does not appear as a peak in the Mn *K*-edge pre-edge because the Mn is at the point of the inversion symmetry. However, the hole localization on O $2p$ alters the Mn $3d$ hole occupation number, which manifests itself as a small decrease in the integrated intensity of the pre-edge. The character of the atomic distortions[33] is consistent with charge ordering on the O sites rather than on the Mn sites, as we discussed in Sec. VI C. These results imply a $2p$ character of the doped states in $La_{0.33}Ca_{0.67}MnO_3$, indicating that this compound is still in the CT state and that the basis (6), ignoring the O $2p$ states, is not tenable. It is also very unlikely that, being of CT type at $x=0$ and 0.67, $La_{1-x}Ca_xMnO_3$ would turn out to be of MH type in the intermediate compounds. Indeed, a proportional increase of the first peak in the O *K* edge is not accompanied by any discernible changes in the $L_{3,2}$ edge spectra within the EELS energy resolution.[18] Higher-resolution Mn $L_{3,2}$ XANES measurements[20] of $La_{1-x}Sr_xMnO_3$ ($x=0.18$–0.4) show a very small *decrease* of the total Mn L_3 count as x goes from 0.18 to 0.4 that is not completely understood yet. In any case, combining the analysis of the O *K*- with the Mn L_3-edge data[18,20] provides supporting evidence for the p character of doped carriers, disfavoring the restricted basis (6).

The basis (5) satisfied a broad range of experimental observations including the present XANES study, although it is

much more complex. This problem has not been solved for the manganites so far, as far as we know. That is also not a purpose of this paper, other than to point out two endemic properties of the Mn $3d$–O $2p$ hybridization, stimulate a wider discussion on the issue, and appeal to further experiments in this direction. First, there is no unique ''intermediate'' Mn state in manganites as was proposed earlier.[27] The Mn valence may be understood as a mixture of many-body electronic configurations with an essential O $2p$ component over the ground state, and, therefore, the CMR materials should be viewed as charge-transfer-type insulators in a broad range of doping. Secondly, hybridization in strongly correlated compounds is not merely an electronic (or spectroscopic) issue. It is a *local effect* governed by competition between the different CT many-body electronic configurations coupled with spin and lattice degrees of freedom. We expect that the problem [Eq. (5)] might be essentially simplified by imposing constraints on the possible local distortions and local magnetic ordering as they are derived from measurements. The former would be accessible through detailed EXAFS and neutron-diffraction PDF analyses that would be able to reconstruct a realistic Mn-O pair distribution function. The latter would be possible from NMR and muon spin-rotation measurements. Contact with experimental data will lead to a better understanding of local energy balances and effective interactions between the carriers in the manganites.

VII. CONCLUSION

We have reported a study of the Mn K edge of $La_{1-x}Ca_xMnO_3$ CMR materials, considering three pair correlations, according to the three fundamental degrees of freedom governing the unusual electronic properties of manganites, namely, the electronic structure of the unoccupied states probed by the Mn K-edge profile vs (i) local atomic distortions; (ii) local magnetic ordering; and (iii) the charge-transfer nature of the Mn-O bonds. The calculations are accompanied by Mn K-edge XANES measurements in the temperature range 30–300 K.

The Mn K edge in $La_{1-x}Ca_xMnO_3$ is dominated by the dipole $1s \rightarrow 4p$ transition. The main features at the absorption edge can be qualitatively reproduced in terms of single-electron MS calculations for a large cluster of atoms. The main edge profile is found to be very sensitive to distortions of the MnO_6 octahedra as x goes from 0 to 1. Lattice polaronic distortions in $La_{0.7}Ca_{0.3}MnO_3$ can be simulated by assuming a strongly distorted orthorhombic structure above and an almost undistorted rhombohedral structure below T_c.

To simulate the effects of magnetic ordering in $x=0$, 0.3, and 1 compounds we have developed a local magnetic moment matching approach, relying on knowledge of the magnetic structure of the compounds. Although several approximations are made in the calculations, the spin-polarized PDOS's of d-type of $LaMnO_3$ and $CaMnO_3$ agree reasonably well with results of self-consistent LDA calculations.[43] Spin-dependent scattering of the photoelectron in the final state results in an energy shift between the majority- and minority-spin spectra that contributes to the total XANES broadening below the Néel (Curie) temperature. The energy shift reaches a maximum of 1.1 eV in the metallic $x=0.3$ sample. In $LaMnO_3$ and $CaMnO_3$ it is found to be ~ 0.9 and ~ 0.5 eV, respectively. We anticipate that experimental Mn K-edge SPXANES will be reported soon which would open the way for direct comparison of calculated and measured spectra.

A small feature B_3 at approximately 6 eV above the main absorption peak is beyond the scope of single-electron calculations including spin-polarized ones. It should be assigned to a shake-up transition. A genuinely many-body approach for calculations of the excitation spectrum has been developed and successfully tested. The inclusion of $S(\omega)$ introduces additional broadening, rescales the absolute energy, and improves the overall agreement, in particular, giving rise to the shake-up peak B_3. We investigate the charge-transfer vs Mott-Hubbard-type ground state using the U_d, Δ, and T_{dp} parameters as determined by previous Mn $2p$ x-ray photoemission spectroscopy measurements[22,48] and find that $LaMnO_3$ should be viewed as a CT-type insulator with a substantial O $2p$ component in the ground state.

The relative orders of magnitude of the three effects governing the Mn K-edge profile are established. Charge transfer in the Mn-O system has the largest impact on the shape of the Mn K edge compared to the results of the conventional single-electron MS calculation. It leads to corrections in the energy scale larger than 6 eV with 14% of the spectral weight transferred to the higher-energy satellite peaks in $LaMnO_3$. Local structure distortions in $LaMnO_3$ can bring about a 1.5 eV spectral weight redistribution if one considers the transition from fully developed JT distortions to an almost undistorted structure. The smallest of the three, the local magnetic ordering, manifests itself as ~ 1.1 eV splitting of the Mn $4p$ states in the $x=0.3$ sample.

In light of these findings the controversial issue of the Mn valence states in the manganites is critically reexamined. The model implying ''intermediate'' Mn valence[27] is clearly oversimplified: it has no potential to reproduce the shake-up feature in the Mn K-edge XANES and rich satellite structure in the Mn $2p$ XPS spectra. It assumes a gradual hole filling on Mn $3d^4$ states upon doping, inconsistent with O K- and Mn $L_{3,2}$-edge measurements.[18,20] Finally, it seems to be difficult to reconcile a single Mn valence with observations of CO states for $0.5<x<0.7$,[3,4] and different types of MnO_6 octahedra across T_c,[26] or T_{CO}.[4,33] The widely accepted model assuming a mixture of Mn $3d^3$ and Mn $3d^4$ with different numbers of holes at the Mn sites depending on local lattice distortions and local magnetic ordering, or in a wider sense, the Mott-Hubbard-type of ground state, in manganites removes many but not all of the above questions. In particular, the $3d$ character of the ground state contradicts the O K- and Mn $L_{3,2}$-edge EELS.[18] In the framework of Mn K-edge spectroscopy, the MH-type model cannot describe the shake-up peak in $LaMnO_3$ and the unusual temperature dependence of the pre-edge peak in $La_{0.33}Ca_{0.67}MnO_3$. The logical consequence of this model would be hole localization on the Mn $3d$ orbitals below T_{CO} implying an increase of the Mn $3d$ occupation number that is not observed experimentally by our Mn K-edge measurements. A small reduction of

the integral intensity of the pre-edge peak indicates a decrease of the Mn $3d$ occupation number at $T<T_{CO}$ and, therefore, a predominant hole localization on the O $2p$ orbitals. We argue that the disproportionation may be understood as a mixture of charge-transfer many-body electronic configurations coupled with spin and lattice degrees of freedom, expression (5). This approach would explain the shake-up peak in the Mn *K*-edge XANES of $La_{1-x}Ca_xMnO_3$ as well as the unusual temperature dependence of the pre-edge feature in $La_{0.33}Ca_{0.67}MnO_3$. It satisfies a wide range of experimental observations, including spectroscopic,[18,20,22] transport,[18] and structural data.[4,13,33] From a practical point of view, only three configurations seem to contribute to the ground state of $LaMnO_3$ ($\gamma_2\sim0.5$, $\gamma_3\sim0.4$, and $\gamma_4\sim0.1$) and $CaMnO_3$ ($\gamma_5\sim0.4$, $\gamma_6\sim0.5$, and $\gamma_7\sim0.1$).[22] Which configurations are essential in doped manganites still remains a question to be examined both theoretically and experimentally. The success of the present simple pair correlation analysis indicates that Mn *K*-edge x-ray absorption near edge structure spectroscopy is a promising tool to study the electronic structure of the unoccupied states of complex materials.

ACKNOWLEDGMENTS

This work was supported in part by the Consortium for Advanced Radiation Source, University of Chicago, and the National Science Foundation Grant No. DMR-9733862. Data acquisition was done at the National Synchrotron Light Source, Brookhaven National Laboratory, which is supported by the U. S. Department of Energy, Division of Materials Sciences and Division of Chemical Sciences, under Contract No. DE-AC02-98CH10886.

*Corresponding author. Present address: Department of Physics, New Jersey Institute of Technology, Newark, NJ 07102.

[1] G.H. Jonker and J.H. van Santen, Physica (Amsterdam) **16**, 337 (1950).
[2] E.O. Wollan and W.C. Koehler, Phys. Rev. **100**, 545 (1955).
[3] A.P. Ramirez, P. Schiffer, S.-W. Cheong, C.H. Chen, W. Bao, T.T.M. Palstra, P.L. Gammel, D.J. Bishop, and B. Zegarski, Phys. Rev. Lett. **76**, 3188 (1996).
[4] P.G. Radaelli, D.E. Cox, M. Marezio, and S.-W. Cheong, Phys. Rev. B **55**, 3015 (1997).
[5] C. Zener, Phys. Rev. **82**, 403 (1951).
[6] P.W. Anderson and H. Hasegawa, Phys. Rev. **100**, 675 (1955).
[7] P.G. de Gennes, Phys. Rev. **118**, 141 (1960).
[8] A.J. Millis, P.B. Littlewood, and B.I. Shraiman, Phys. Rev. Lett. **74**, 5144 (1995).
[9] A.J. Millis, B.I. Shraiman, and R. Mueller, Phys. Rev. Lett. **77**, 175 (1996); A.J. Millis, R. Mueller, and B.I. Shraiman, Phys. Rev. B **54**, 5405 (1996).
[10] G. Zhao, K. Conder, H. Keller, and K.A. Mueller, Nature (London) **381**, 676 (1996).
[11] M. Jaime, H.T. Hardner, M.B. Salamon, M. Rubinstein, P. Dorsey, and D. Emin, Phys. Rev. Lett. **78**, 951 (1997).
[12] C.H. Booth, F. Bridges, G.H. Kwei, J.M. Lawrence, A.L. Cornelius, and J.J. Neumeier, Phys. Rev. B **57**, 10 440 (1998).
[13] A. Lanzara, N.L. Saini, M. Brunelli, F. Natali, A. Bianconi, P.G. Radaelli, and S.-W. Cheong, Phys. Rev. Lett. **81**, 878 (1998).
[14] D. Louca, T. Egami, E.L. Brosha, H. Röder, and A.R. Bishop, Phys. Rev. B **56**, R8475 (1997).
[15] H. Röder, J. Zang, and A.R. Bishop, Phys. Rev. Lett. **76**, 1356 (1996).
[16] M.F. Hundley, M. Hawley, R.H. Heffner, Q.X. Jia, J.J. Neumeier, J. Tesmer, J.D. Thompson, and X.D. Wu, Appl. Phys. Lett. **67**, 860 (1995).
[17] W.E. Pickett and D.J. Singh, Phys. Rev. B **53**, 1146 (1996).
[18] H.L. Ju, H.-C. Sohn, and K.M. Krishnan, Phys. Rev. Lett. **79**, 3230 (1997).
[19] J.-H. Park, C.T. Chen, S-W. Cheong, W. Bao, G. Meigs, V. Chakarian, and Y.U. Idzerda, Phys. Rev. Lett. **76**, 4215 (1996).
[20] E. Pellegrin, L.H. Tjeng, F.M.F. de Groot, R. Hesper, G.A. Sawatzky, Y. Moritomo, and Y. Tokura, J. Phys. IV **7**, C2-405 (1997).
[21] J. Zaanen, G.A. Sawatzky, and J.W. Allen, Phys. Rev. Lett. **55**, 418 (1985).
[22] T. Saitoh, A.E. Bocquet, T. Mizokawa, H. Namatame, A. Fujimori, M. Abbate, Y. Takeda, and M. Takano, Phys. Rev. B **51**, 13 942 (1995).
[23] See, for example, T.A. Tyson, Q. Qian, C.-C. Kao, J.-P. Rueff, F.M.F. de Groot, M. Croft, S.-W. Cheong, M. Greenblatt, and M.A. Subramanian, Phys. Rev. B **60**, 4665 (1999), and references therein.
[24] The final states measured by XANES are not the ground states of the electronic system due to the hole-induced excitonic shift of the valence band. The final states are discussed in terms of two static limits: the Z and $Z+1$ approximations. See also Ref. 36.
[25] A.J. Millis, Nature (London) **392**, 147 (1998).
[26] A. Lanzara, F. Natali, N.L. Saini, A. Bianconi, and P.G. Radaelli, J. Synchrotron Radiat. **6**, 776 (1999).
[27] G. Subías, J. García, M.G. Proietti, and J. Blasco, Phys. Rev. B **56**, 8183 (1997).
[28] F. Bridges, C.H. Booth, G.H. Kwei, J.J. Neumeier, and G.A. Sawatzky, Phys. Rev. B **61**, R9237 (2000).
[29] M. Croft, D. Sills, M. Greenblatt, C. Lee, S.-W. Cheong, K.V. Ramanujachary, and D. Tran, Phys. Rev. B **55**, 8726 (1997).
[30] Q. Qian, T.A. Tyson, C.-C. Kao, M. Croft, S.-W. Cheong, and M. Greenblatt, Phys. Rev. B **62**, 13 472 (2000).
[31] J.A.M. van Roosmalen and E. Cordfunke, J. Solid State Chem. **110**, 113 (1994).
[32] A.C. Larson and R.B. Von Dreele, Los Alamos Internal Report No. 86-748, 1985–1990 (unpublished).
[33] M.R. Ibarra, J.M. De Teresa, J. Blasco, P.A. Algarabel, C. Marquina, J. Garcia, J. Stankiewicz, and C. Ritter, Phys. Rev. B **56**, 8252 (1997).
[34] L. Tröger, D. Arvanitis, K. Baberschke, H. Michaelis, U. Grimm, and E. Zschech, Phys. Rev. B **46**, 3283 (1992).
[35] Q. Huang, A. Santoro, J.W. Lynn, R.W. Erwin, J.A. Borchers, J.L. Peng, and R.L. Greene, Phys. Rev. B **55**, 14 987 (1997).
[36] U. von Barth and G. Grossmann, Phys. Rev. B **25**, 5150 (1982).
[37] P.J. Durham, J.B. Pendry, and C.H. Hodges, Comput. Phys. Commun. **25**, 193 (1982).

[38] H. Ebert, P. Strange, and B.L. Gyoffy, J. Appl. Phys. **63**, 3055 (1988).
[39] Notice that it is the Mn $3p$ core-level splitting due to the exchange interaction with Mn $3d$ band that makes it possible to measure SPXANES by collecting fluorescent $K\beta$ doublet data.
[40] U. von Barth and L. Hedin, J. Phys. C **5**, 1629 (1972).
[41] T.A. Tyson, Phys. Rev. B **49**, 12 578 (1994).
[42] A.L. Ankudinov, B. Ravel, J.J. Rehr, and S.D. Conradson, Phys. Rev. B **58**, 7565 (1998).
[43] S. Satpathy, Z.S. Popović, and F.R. Vukajlović, Phys. Rev. Lett. **76**, 960 (1996).
[44] I.S. Elfimov, V.I. Anisimov, and G.A. Sawatzky, Phys. Rev. Lett. **82**, 4264 (1999).
[45] Y. Okimoto, T. Katsufuji, T. Ishikawa, A. Urushibara, T. Arima, and Y. Tokura, Phys. Rev. Lett. **75**, 109 (1995).
[46] R.V. Vedrinskii, V.L. Kraizman, A.A. Novakovich, P.V. Demekhin, S.V. Urazhdin, B. Ravel, and E. Stern, J. Phys. IV **7**, C2-107 (1997).
[47] A.E. Bocquet, T. Mizokawa, T. Saitoh, H. Namatame, and A. Fujimori, Phys. Rev. B **46**, 3771 (1992).
[48] A. Chainani, M. Mathew, and D.D. Sarama, Phys. Rev. B **47**, 15 397 (1993).
[49] K. Yonemitsu, A.R. Bishop, and J. Lorenzana, Phys. Rev. B **47**, 8065 (1998).
[50] G.D. Mahan, in *Solid State Physics*, edited by H. Ehrenreich, F. Seitz, and D. Turnbull (Academic, New York, 1974), Vol. 29, p. 75.
[51] Z. Shen, J.W. Allen, J.J. Yeh, J.-S. Kang, W. Ellis, W. Spicer, I. Lindau, M.B. Maple, Y.D. Dalichaouch, M.S. Torikachvili, and J.Z. Sun, Phys. Rev. B **36**, 8414 (1987).
[52] H. Tolentino, M. Medarde, A. Fontaine, F. Baudelet, E. Dartyge, D. Guay, and G. Tourillon, Phys. Rev. B **45**, 8091 (1992).
[53] A.S. Alexandrov and A.M. Bratkovsky, Phys. Rev. Lett. **82**, 141 (1999).
[54] A.Yu. Ignatov, J. Synchrotron Radiat. **6**, 532 (1999).
[55] T. Egami, S. Ishihara, and M. Tachiki, Science **261**, 1307 (1993); S. Ishihara, M. Tachiki, and T. Egami, Phys. Rev. B **49**, 16 123 (1994).
[56] Generalization of SPXANES and DANES for strongly correlated compounds is not straightforward. See, for example, X. Wang *et al.*, Phys. Rev. B **56**, 4553 (1997) for x-ray photoemission, and for DANES; L. B. Sorensen *et al.*, in *Resonant Anomalous X-Ray Scattering: Theory and Applications*, edited by G. Materlik, C. J. Sparks, and K. Fischer (North-Holland, Amsterdam, 1994), pp. 389-420, Sec. 9.4.1.